



# Deep learning and LiDAR integration for surveillance camera-based river water level monitoring in flood applications

Nur Atirah Muhadi<sup>1,2</sup> · Ahmad Fikri Abdullah<sup>1,2,3</sup> · Siti Khairunniza Bejo<sup>1,2,4</sup> · Muhammad Razif Mahadi<sup>1,2</sup> · Ana Mijic<sup>5</sup> · Zoran Vojinovic<sup>6</sup>

Received: 15 May 2023 / Accepted: 14 February 2024 / Published online: 21 April 2024  
© The Author(s), under exclusive licence to Springer Nature B.V. 2024

## Abstract

Recently, surveillance technology was proposed as an alternative to flood monitoring systems. This study introduces a novel approach to flood monitoring by integrating surveillance technology and LiDAR data to estimate river water levels. The methodology involves deep learning semantic segmentation for water extent extraction before utilizing the segmented images and virtual markers with elevation information from light detection and ranging (LiDAR) data for water level estimation. The efficiency was assessed using Spearman's rank-order correlation coefficient, yielding a high correlation of 0.92 between the water level framework with readings from the sensors. The performance metrics were also carried out by comparing both measurements. The results imply accurate and precise model predictions, indicating that the model performs well in closely matching observed values. Additionally, the semi-automated procedure allows data recording in an Excel file, offering an alternative measure when traditional water level measurement is not available. The proposed method proves valuable for on-site water-related information retrieval during flood events, empowering authorities to make informed decisions in flood-related planning and management, thereby enhancing the flood monitoring system in Malaysia.

**Keywords** Flood disaster · Deep learning · Image segmentation · LiDAR · Surveillance camera · Water level

## 1 Introduction

Floods are the most frequent type of disaster, causing loss of human lives and damage to properties. Between 2000 and 2019, around 104,600 people were killed and nearly 1.65 billion people were affected by flood events worldwide (UNDRR 2020). Researchers and practitioners have difficulties in finding optimal flood management strategies due to rapid urbanization, population growth, and climate change (Mynett and Vojinovic 2009; Price and Vojinovic 2008; Sathish Kumar et al. 2013). In Malaysia, the Department of Drainage and Irrigation (DID) is responsible for monitoring floods and providing flood forecasting and warning services to the public. Currently, real-time information on rainfall and river

water levels that are available at [publicinfobanjir.water.gov.my](http://publicinfobanjir.water.gov.my), an official website for DID to disseminate flood information, is obtained from remote telemetry units (RTUs) across Malaysia (CFE-DM 2019). A water level sensor is a device that measures river water level and conveys the signal to the RTU to be recorded as a water level reading (DID 2018) before sending it to the state server and then transmitted to the InfoBanjir database. Data unavailability due to transmission or technical problems during flood events may cause interruptions and reduce the effectiveness of the flood monitoring system. Recently, surveillance technology was proposed to be used in flood studies (Akiyama et al. 2020; Lo et al. 2015b, a; Moy de Vitry et al. 2019a, b), especially for the flood monitoring system. Nonetheless, there is a lack of studies that discuss the practical application of surveillance cameras.

Before performing further analysis by surveillance images, the water region that is present in the images is the key information for flood-related applications. Computer vision is the common approach used in this situation that employs a visual sensor to capture and process static images or video streams for flood disaster applications (Arshad et al. 2019; Costa et al. 2013). In the past years, classical computer vision segmentation methods, such as thresholding, edge-based, region-growing, and hybrid techniques were used to separate the water region from the background (Muhadi et al. 2020; Witherow et al. 2018). Although these segmentation algorithms could detect the water regions, the main drawback of these methods is that it is handcrafted only for specific data that they were created with (Lopez-Fuentes et al. 2017; Muhadi et al. 2020). Since the deep learning approach offers more robust and generic applications, researchers and experts have been interested in exploiting deep learning in their studies. The evolution of convolutional neural networks (CNN) in deep learning has piqued their curiosity, as CNN provides excellent accuracy outcomes with minimal human interventions.

Recent research has highlighted the potential of deep learning and neural network applications in flood management. Bentivoglio (2021) and Khouakhi (2022) both emphasize the need for more open and labeled flood image datasets to advance the use of convolutional neural networks (CNNs) in flood extent detection and flood depth estimation. Bui (2019) and Hashemi-Beni (2021) have demonstrated the effectiveness of deep learning models in predicting flash flood susceptibility and mapping flood extent, respectively. These collective findings emphasize the critical role of data accessibility and highlight the promising potential of deep learning in enhancing flood management strategies. Recent studies have demonstrated the potential of deep learning in flood surveillance applications. Chopde (2022) utilized deep learning techniques to identify flooded areas and observe water levels, respectively. Munawar (2021) further extended this by developing a real-time flood management system using unmanned aerial vehicles and deep learning algorithms. Nair (2021) proposed a machine vision-based flood monitoring system that uses deep learning and fuzzy logic to detect and estimate flood depths, based on crowdsourced image data. These studies collectively highlight the effectiveness of deep learning in enhancing the accuracy and efficiency of flood applications.

In the realm of utilizing surveillance cameras, Lopez-Fuentes et al. (2017) applied deep learning algorithms to identify flooded locations. This was done within the framework of flood investigations, showcasing the effective use of advanced technology in extracting relevant information from surveillance camera footage. The authors used FCN-8 s, DenseNet, and Pix2Pix segmentation networks and investigated the effectiveness of each network. In addition, Moy de Vitry et al. (2019a, b) proposed a floodwater detection system based on a fine-tuned U-net design. It was reported that the results of intersection-over-union (IoU) were higher than 90% on average. Akiyama et al. (2020) did similar work by training

a segmentation model based on the SegNet network. The authors set up the camera in a specific position and utilised photos taken for 50 days as training data to segment water from the same river. The performance was evaluated using pixel accuracy and IoU metrics and the results were high, achieving over 97%. The same team conducted a comprehensive investigation into two different CNN networks, SegNet and FCN (Eltner et al. 2021). Both networks produced similar results, however, SegNet achieved slightly higher accuracy than FCN. However, the authors only used images from the study area as a training dataset and then applied the trained models to the images from the same location. Then, Vandaele et al. (2021a, b) compared the performance of DeepLabV3 and UperNet networks, concluding that DeepLabV3 achieved better performance. Based on the results, this study adopted Deeplabv3+ to carry out the segmentation process to identify water regions in the surveillance images. The segmentation results were then used to estimate the river water level.

In terms of water level, only a few studies did not use the scale on stick gauge or dimensions of objects as references when conducting work to determine the water level, specifically when surveillance cameras were used. Lo et al. (2015b, a) defined pre-labelled markers that represented the actual boundaries of the riverbank. By identifying the proportion of virtual markers covered by the water body, the result reflected the extent of water overflow. Nevertheless, this method could not give absolute water level values. Then, Moy de Vitry et al. (2019a, b) introduced a qualitative flood index known as the scalable observer flood index (SOFI) that acted as a proxy for water level fluctuations. SOFI was used by calculating the proportion of the flooded pixels to the total number of pixels of either a defined region of interest (ROI) or the whole image. The approach, however, did not directly estimate the water level but instead studied the fluctuation of water level over time. Next, Vandaele et al. (2021a, b) proposed an algorithm known as landmark-based water-level estimation (LBWLE) that used the heights of landmarks from sea levels to estimate the water level. However, LBWLE required landmark information which sometimes is not available in certain areas. The necessity of relying on stick gauges or objects found on-site may limit the practicality. Furthermore, high-quality photos are needed in order to capture the scale or object information. To address these constraints, the study suggests an inventive solution. It involves employing virtual markers enriched with elevation data obtained from LiDAR technology to estimate water levels, leveraging the results of surveillance image segmentation. This approach aims to overcome the limitations associated with conventional methods of water level estimation.

Additionally, a 3D model was also developed by integrating the LiDAR data and river dimension measured on the field to have better visualisation during a flood disaster. Having a 3D visualisation technique could improve the interpretation ability of disaster data and the efficiency of decision-making processes (Costabile et al. 2021). Besides, combining the 3D model with the estimated water level could determine the water volume of the study area. In flood applications, the detected flood input has a significant impact on emergency response time (Oddo and Bolten 2019). Delays in flood response could increase the risk and cause huge impacts.

Therefore, a specific application designed for monitoring and managing flood disasters is needed to provide a quick response, especially during flood events. The novelty of this study lies in addressing the limitations associated with traditional flood monitoring methods. The reliance on stick gauges or on-site objects, often requiring high-quality photos, poses practical constraints. To overcome these limitations, this research proposes an innovative approach using virtual markers with elevation information extracted from LiDAR data for water level estimation based on surveillance image segmentation results. This novel methodology is particularly relevant in the context of flood disasters, where a rapid

response is crucial. The study introduces a specific application designed for flood monitoring and management, integrating surveillance technology and deep learning. By combining water segmentation and water level estimation through deep learning semantic segmentation, the research establishes a robust flood monitoring system. Furthermore, the incorporation of predefined virtual markers, enriched with elevation data from LiDAR, enhances the accuracy and practicality of water level estimation. The ability to record information in an Excel file adds a layer of utility, providing an alternative measure for water level monitoring in situations where conventional methods prove impractical. The integration of surveillance technology, deep learning, and LiDAR data, as demonstrated in this study, not only offers a novel and effective flood monitoring system but also proves invaluable during flood events. The development of a graphical user interface (GUI) further streamlines the process, allowing for the extraction and storage of water-related information in a database. This database can then be leveraged for improved flood management and planning, emphasizing the comprehensive and forward-thinking nature of this innovative work.

## 2 Methodology

### 2.1 Study area

Images from a surveillance camera installed by the Department of Irrigation and Drainage (DID), Malaysia were used to investigate the efficiency of the deep learning approach in extracting the water region information. DID surveillance cameras were installed near the river, which allowed the authority to monitor the real situation on-site. The images were retrieved from the DID Selangor official website as a platform to convey real-time flood information to the public. In this study, images captured at different times and days were used for water detection using the deep learning semantic segmentation method at one of the DID stations at Sungai Bernam in Kampung Selisek as shown in Fig. 1. The station was also equipped with a water level sensor to validate the performance of the estimated water level proposed by this work.

### 2.2 Water segmentation procedure using a deep learning approach

The first processing step to extract information from the surveillance image was the segmentation of the water features. A deep learning semantic segmentation algorithm was used to classify each pixel in the image into water and background classes. The process of training a semantic segmentation network to classify images involves several procedures such as preparing a collection of pixel-labelled images, training the network, and assessing the accuracy of the network. All processing steps were performed using MATLAB 9.10 (R2021a) on a notebook equipped with a 2.60 GHz Intel® Core™ i7 CPU and 16 GB RAM.

In this study, around 1,011 water-related images were collected from global and local scenes to reflect various water scenarios and scene representations for preparing the training dataset. The segmentation network was trained using DeepLabv3+ architecture. It was trained using stochastic gradient descent with momentum (SGDM) of 0.9 with a value of 0.005 for L2 regularisation. The learning rate was reduced from an initial value of 0.0003 by a factor of 0.3 every 10 epochs. A mini-batch with eight observations for each iteration was used and the model was trained for up to 30 epochs. Further information on the water



**Fig. 1** An example of the image from DID surveillance camera in the study area

segmentation procedure has been discussed by Muhadi et al. (2021). Figure 2 illustrates the overall deep learning workflow of this study.

### 2.3 Segmentation evaluation

The results from the segmentation process were evaluated to assess the ability of the algorithm to segment the surveillance images. Nonetheless, the evaluation task was not included in the GUI. The segmentation evaluation was carried out using the intersection-over-union (IoU) metric. The IoU metric is one of the most frequent evaluation metrics used to assess segmentation performance. It was computed by calculating the area of overlap between the predicted segmentation and ground truth divided by the encompassed area of both predicted and ground truth data. The IoU ranges from 0 to 1, whereby 1 indicates a full overlap between both data, and 0 demonstrates no overlap between predicted and ground truth data. The IoU metric can be defined in Eq. (1):

$$IoU = \frac{S_i \cap G_i}{S_i \cup G_i} \quad (1)$$

Given  $S_i$  is the segmentation and  $G_i$  is the ground truth of image  $i$ .

### 2.4 River water level estimation procedure

#### 2.4.1 Estimation of river water level

The segmented images from the previous task were used to measure water level estimation in this proposed work. Before performing water level estimation, a post-processing stage was

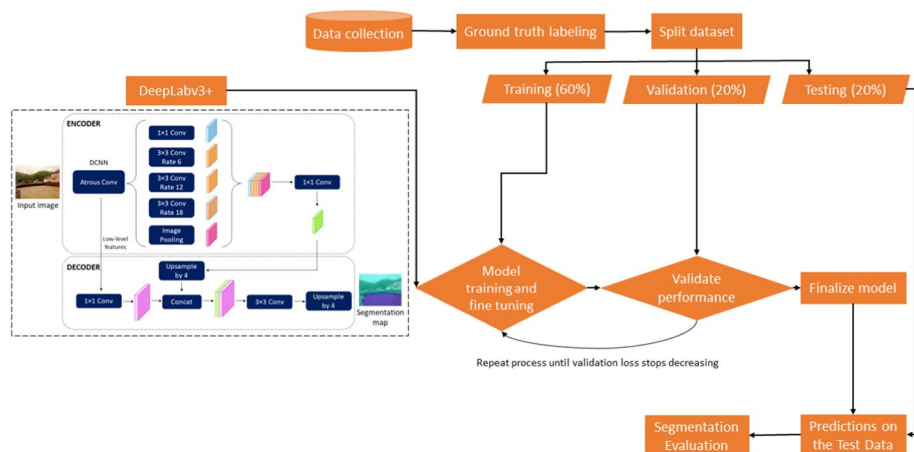


**Fig. 2** The workflow of the deep learning method

carried out on the segmentation results to enhance the water features. The results were converted into a binary image and then the first morphological operation was performed. Small objects that have fewer than 100,000 pixels were removed from the image, leaving only a big connected water feature and removing noises. A morphological close operation was carried out to smooth the outline and close any open holes near the borders that were specified at a radius of 2 pixels. Lastly, a flood-fill operation was performed to fill holes in the background of the binary images. Therefore, irrelevant artefacts could be removed from the images. The post-processed segmentation images were then integrated with virtual markers to estimate water level values.

Several virtual markers with elevation values were identified in the image beforehand. Since it requires to have prior elevation information, the water level estimation procedure was highly dependent on locality. In this study, terrestrial light detection and ranging (LiDAR) data were used to generate a high-resolution digital elevation model (DEM) to acquire elevation information for estimating the surface water level of the river. LiDAR data was acquired using FARO Laser Scanner Focus3D X 130 to capture the surroundings of the river. A cell size of  $1 \times 1$  LiDAR-derived DEM was generated using the ArcGIS 10.2.2 software. In the ArcGIS environment, the elevation data for the marker locations were obtained using the Extract Values to Points function, which is one of the Spatial Analyst tools. The elevation values of the provided markers were combined with the positions of the specified markers that were previously detected from surveillance photos.

The post-processed segmentation results were then overlaid with the elevation value of the markers to characterise the depth of water level of a given image. To improve water level estimation, water level markers should be located outside the river, in an area where segmentation errors are less common, boosting the estimation accuracy. The pixel value of markers from the binary image was determined, with 1 representing the water region and 0 representing the background image. The water level was calculated using the mean elevation values of the last two markers that obtained pixel values of 1 and 0.

The DID introduces water level thresholds, which include the normal level, alert level, warning level, and danger level, to describe the severity of river water levels. Depending on river water levels, the threshold values differed at each station. Table 1 shows the water level threshold values for Kg. Selisek. The information from Table 1 was used in identifying the water level status from the estimated water level.

**Table 1** Water level threshold values for Kg. Selisek

| Status  | Water level (m) |
|---------|-----------------|
| Normal  | 23.0            |
| Alert   | 26.1            |
| Warning | 26.6            |
| Danger  | 27.1            |

While the segmentation procedure demonstrates versatility across diverse flood scenarios, a noteworthy constraint within the proposed methodology lies in its locality-based river water level estimation. This limitation emerges from the dependence on elevation values specific to each area. To effectively apply the proposed estimation framework, it is imperative to acquire elevation data tailored to the particular area of interest.

## 2.4.2 Validation of water level estimation

The performance of the water level framework was evaluated to investigate how reliable the estimated water level values were. The assessment of the water level was done by using Spearman's rank-order correlation coefficient (Spearman 1904) to determine the relation between the estimated water level and the water level measured by the sensor on-site. The Spearman's correlation is a nonparametric measure that evaluates a monotonic relation between two sets of continuous or ordinal data. Both water levels were ranked, and the lowest value was assigned with the smallest rank. Since two or more items were repeated (tied rank) in this study, Eq. (2) was used for computing rank correlation to measure the strength of a monotonic relation between water level and flood index.

$$\rho = 1 - 6 \left[ \frac{\sum D^2 + \frac{m_i^3 - m_i}{12} + \dots}{n(n^2 - 1)} \right] \quad (2)$$

where  $m_i$  is the number of repetitions of  $i^{th}$  rank. The Spearman's correlation value can vary between -1 to 1, in which 1 indicates a perfect positive association of the variables, 0 indicates no relation exists between the variables, and -1 expresses a perfect negative relation. The closer the correlation value is to  $\pm 1$ , the stronger the monotonic relation.

Besides, the performance metrics were also carried out by comparing the water level framework with readings from the sensors to validate the proposed water level outputs by using the mean absolute error (MAE) and root-mean-square error (RMSE). MAE is a measure of the average absolute difference between predicted water levels and observed values meanwhile, RMSE investigates how deviate the estimated values from the observed values. MAE and RMSE can be calculated using Eq. (3) and (4).

$$MAE = \frac{1}{n} \sum_{i=1}^n |\hat{y} - y| \quad (3)$$

$$RMSE = \sqrt{\sum_{i=1}^n \frac{(\hat{y} - y)^2}{n}} \quad (4)$$

where  $\hat{y}$  represents the estimated water level and  $y$  is the observed water level.



In addition, the study includes descriptive statistics—a crucial component of data analysis that provides a succinct summary of a dataset's key characteristics. In the context of water level estimation, a set of water level estimations has been subject to various statistical measures. These measures provide valuable insights into the distribution, central tendency, and variability of the estimations. The minimum and maximum values delineate the range of estimations, quartiles and the median offer information on distribution, while the mean serves as an average estimation. Additionally, variance and standard deviation quantify the variability within the dataset. The ensuing descriptive statistics table provides a comprehensive snapshot of the essential features of the water level estimations, aiding in the interpretation and contextualization of the dataset.

## 2.5 Visualisation of water level using a 3D model

A 3D model of the study area was developed as a topographic representation for better visualisation during flood disasters. The river dimensions and the DEM derived from LiDAR were combined to create the 3D model. To illustrate the fluctuation of water levels visually, the 3D model was overlaid with the estimated water levels from the proposed work. Additionally, the suggested concept was also used to calculate the water volume.

The raw LiDAR data was converted into a DEM raster by using natural neighbour interpolation. The dimensions of the river, in terms of river width and riverbed information, were fused with the DEM data to resemble the actual river condition. The river dimensions were manually measured in the field. The average depth of the riverbed was 6.7 m, and the river's width was 10 m. The dimension data and the DEM from LiDAR were combined using the Mosaic function in the ArcGIS software.

The 3D model was then used to observe the changes in the water levels of the river. The simulation was used to represent the rising of the water at various water level values using the estimated water level that was obtained from the analysis in the previous section. Besides, the volume of water could be determined using the 3D model by computing the volume between the area below the surface and a reference plane as shown in Fig. 3. The reference plane refers to the water level estimated from the previous section.

## 2.6 Designing the GUI for water segmentation and water level estimation procedures

In this study, the GUI for the flood monitoring system was developed to help the user retrieve data and extract meaningful information from surveillance images. The proposed GUI consists of two processing steps embedded in it. The first step was the segmentation of the water region using a deep learning approach. Then, the segmentation result was used to measure the water level estimation and identify the water level status on-site. The simple GUI was designed using the App Designer tool in MATLAB® software. App Designer is an interactive development environment for creating and designing an application layout as well as programming app behaviour. The Design View in App Designer is used to layout the user interface of the app. Then, the behaviour of the application was defined using the Code View. The GUI is designed to allow surveillance images to be segmented and water levels to be estimated simultaneously before the information is recorded into a database for further analysis. The designed app used the





**Fig. 3** The surface volume was calculated between the area below the reference plane and the surface of DEM (shaded area)

app packaging tool in Matlab so that users could install the packaged app. The installed app will appear in the Apps tab in the Matlab Toolstrip, hence it can be used by other Matlab users.

There are two elements of the GUI, one for the segmentation process and the other for water level estimation. For the segmentation part, the user interface contains a ‘Load Image’ button that allows the user to load an input image. The application displays the uploaded image in an axis component on the right side of the user interface. The ‘Start’ button on the second panel enables the semantic segmentation process to start executing. The segmentation result appears at the axes component on the right side. At the bottom, there is an export button that allows the user to save the image to the desired file location. Figure 4 shows the layout of the water segmentation procedure.

For water level estimation, the ‘Retrieve’ button would regain the segmented image from the previous process. There is a location option that enables the user to choose the location of the image that would retrieve the virtual markers to estimate the water level. Besides, there are date and time selection buttons to allow the date and time of the image to be recorded and saved into an Excel sheet. The water level estimation button enables the estimation process to be executed. The water level result appears above the image with a status, indicating the severity of the water level. At the bottom, there is an export data panel that allows the user to export the current image display on the axis and water level information. The ‘Segmentation Image’ button enables the user to save the image to a directory chosen by the user. Meanwhile, the export data panel enables the estimated water level to be saved into the Excel sheet in a predefined file location. The Excel file can be used to plot graphs and study the pattern of water level. Figure 5 presents the layout of the water level estimation procedure.

### 3 Results and discussion

#### 3.1 Evaluation of water segmentation using deep learning

Visual assessment of the segmentation results indicated that the proposed segmentation was able to segment the images into water and background regions. The segmentation results and ground truth data overlapped quite well with minor errors near the water boundaries as shown in Fig. 6. The segmentation results were overlaid with the expected ground truth to identify the errors more distinctly as shown in Fig. 6d. The magenta and green-coloured regions are areas that differed from the ground truth which represent FN and FP areas, respectively.

Next, segmentation metrics were carried out over the entire dataset and class-wise assessment. In terms of the entire dataset, the IoU metric achieved around 0.95, indicating a huge overlap between the segmentation image and the ground truth data. Having an outdoor scene often causes imbalanced classes because it is impossible to have a balanced

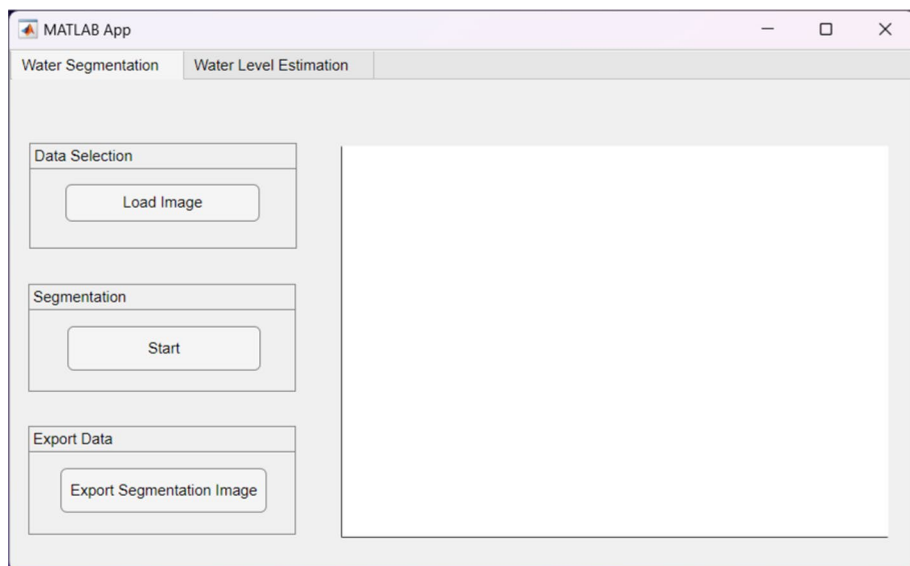


**Fig. 4** The layout of the automated segmentation procedure

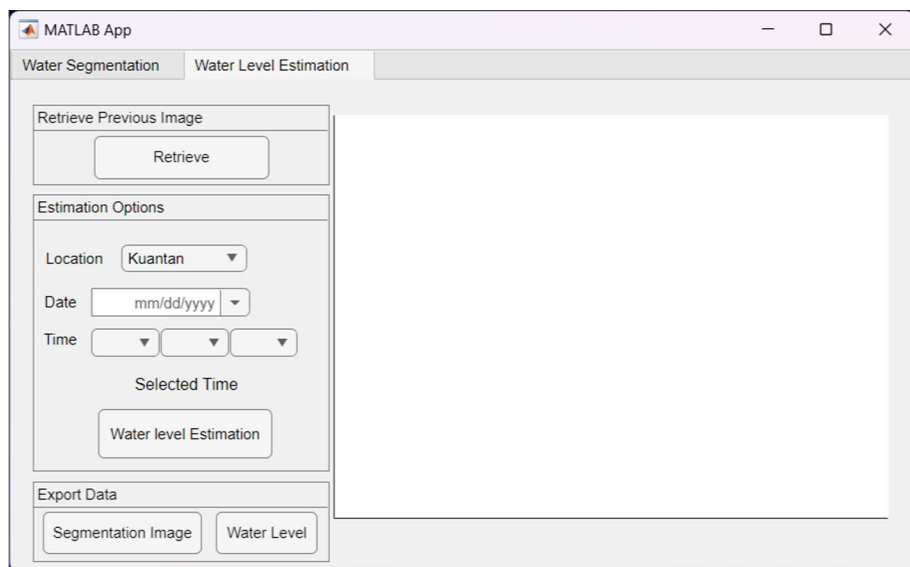


**Fig. 5** The layout of the water level estimation procedure

number of pixels that belong to the foreground (water region) and the background classes. As a result, segmentation metrics were assessed for each class in order to avoid results that were biased by the dominant class (Fernandez-Moral et al. 2018). Table 2 shows the IoU results for both water and background classes.

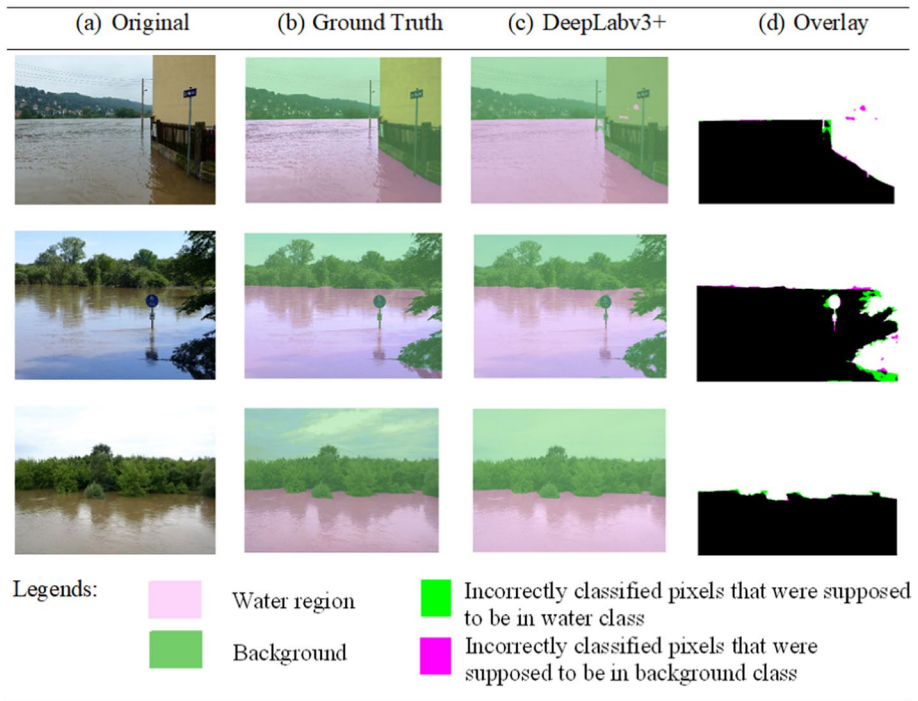


**Fig. 6** Visualization and comparison of representative results on test data. **a** Original image. **b** Ground truth. **c** DeepLabv3+ prediction. Pink and green areas represent water and background regions, respectively. **d** Overlays of ground truth and segmentation results

**Table 2** Per-class metrics of the water segmentation using Deeplabv3+

| Classes    | IoU  |
|------------|------|
| Water      | 0.94 |
| Background | 0.96 |

In terms of class, it clearly showed that background class, which was dominant in the dataset, achieved higher values of segmentation metrics. Overall, Deeplabv3+ scored more than 0.93 for both classes. The results demonstrated that Deeplabv3+ was effective in segmenting water and background regions from the surveillance images. Then, the results from the present work were compared with previous studies done by Lopez-Fuentes et al. (Lopez-Fuentes et al. 2017) and Vandaele et al. (Rémy Vandaele et al. 2021a, b). Both researchers carried out the same concept but used different architecture networks. Lopez-Fuentes et al. employed a fully convolutional network (FCN-8s), fully convolutional DenseNet or also known as Tiramisu, and Pix2Pix networks to detect water areas from images, while Vandaele et al. investigated the performance of DeepLab and UperNet networks.

All studies used a variety of water-related photos, which allowed a fair comparison between the findings. Table 3 shows the comparative results between Deeplabv3+ and other networks from previous studies. Based on the results, Deeplabv3+ achieved the highest value of the IoU metric, demonstrating better capability in segmenting water regions from the images.

**Table 3** A comparison between results obtained from the present work and the previous studies

| Author(s)                   | Segmentation networks | Mean IoU (%) |
|-----------------------------|-----------------------|--------------|
| This work                   | DeepLabv3+            | <b>94.93</b> |
| Vandaele et al. (2021a, b)  | DeepLab               | 93.74        |
|                             | UperNet               | 93.32        |
| Lopez-Fuentes et al. (2017) | Tiramisu              | 81.91        |
|                             | Pix2pix               | 72.25        |
|                             | FCN-8 s               | 70.05        |

### 3.2 Validation of water level estimation

The segmentation results were then exploited to extract the water level information from the images. To ensure that the estimated water levels are reliable, the estimated values were validated by comparing them with the water level measurements observed from the sensor in the study area. Around 76 image data captured at different times and dates were utilised for validation purposes. The following table presents key statistical measures derived from a dataset related to water level estimation. These measures offer insights into the distribution, central tendency, and variability of the estimations. The range between the minimum and maximum values, from 25.05 to 27.10, illustrates the spread of the estimations. Quartiles and the median provide information about the distribution, while the mean offers an average estimation. Variance and standard deviation quantify the variability within the dataset. The detailed statistical summary is presented in Table 4.

The water levels observed from the sensor at particular times and dates were compared with the estimated water level extracted from the images. The relation between the estimated and observed water levels was investigated by using Spearman's rank-order correlation. Besides, the performance metrics such as Mean Absolute Error (MAE) and root-mean-square error (RMSE) of the estimated water level were also computed. The MAE represents the average of the absolute difference between the actual and predicted values in the dataset. It measures the average of the residuals in the dataset, without considering their direction. In this study, the MAE obtained was 0.01, which suggests that the estimated water levels were, on average, very close to the actual values. Meanwhile, RMSE is a measure of the average magnitude of the errors between predicted and observed values. The computed RMSE was 0.86, indicating that the predicted water level values deviate from the observed values by 0.86 m. The Spearman's correlation achieved over 0.92, indicating that there was a strong correlation between the two data. The findings signified that the variations of the estimated water values could describe the water level trends of the river. The estimated water levels could be recorded in a structured database so that the decision-makers could retrieve the data and do further analysis. For instance, the decision-makers can plot a graph using the estimation values and help them visualise the water level pattern on-site. Figure 7 illustrates the pattern of water levels using the proposed water level estimation and water level sensor.

The patterns observed in both methods closely matched the obtained correlation. Despite notable differences at certain points compared to the observed water level, these variations still remained consistent within the same water level status. Consequently, the provided information offers decision-makers a general overview of the river water level condition. It is suggested that including more predefined markers could mitigate errors and enhance the overall efficiency of the approach.

**Table 4** Descriptive statistics of the data

| Statistic                | Water level estimation (m) |
|--------------------------|----------------------------|
| Minimum                  | 25.05                      |
| Maximum                  | 27.10                      |
| 1st Quartile             | 25.05                      |
| Median                   | 26.35                      |
| 3rd Quartile             | 27.10                      |
| Mean                     | 26.26                      |
| Variance (n–1)           | 0.63                       |
| Standard deviation (n–1) | 0.79                       |

In the context of broader scientific literature, the findings underscore the reliability of the proposed methodology for assessing river water levels. However, it is crucial to acknowledge some limitations, such as the need for additional predefined markers to further improve accuracy. This aligns with the broader discourse on enhancing monitoring systems for more precise and reliable results.

Considering the research results, the study recommends feasible policy interventions to optimize flood management strategies. The insights gained from the proposed methodology can inform decision-makers in developing more effective policies for mitigating the impact of floods, thus contributing to the broader field of water resource management and disaster preparedness.

**3.3 Water level fluctuation with the 3D model**

In order to represent the elevation of the river and its surroundings, the 3D model was developed from LiDAR data by combining dimension information from the river and the DEM obtained from LiDAR data. Figure 8a shows the resulting DEM after mosaicking both data that could portray the riverbed as well as the elevations of the surrounding area. Meanwhile, Fig. 8b depicts the cross-section of the river.

Flood simulation was performed to describe the water level changes and to identify water overflows during the rising of the water level. This study adopted the estimated water level from Sect. 2.4.1 to visualise the rising water level in the study area. Figure 9

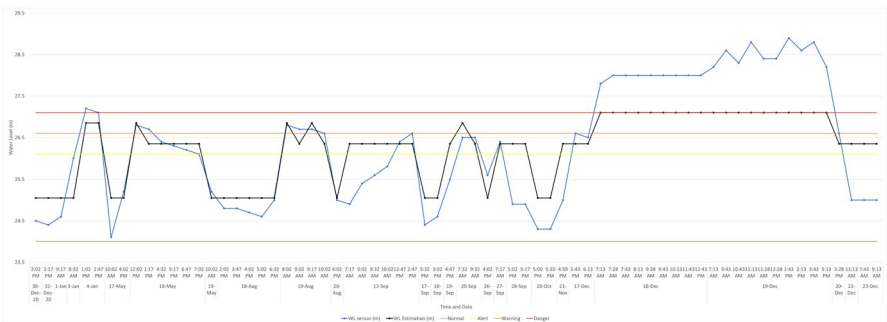


**Fig. 7** The water level pattern of estimated and observed water level

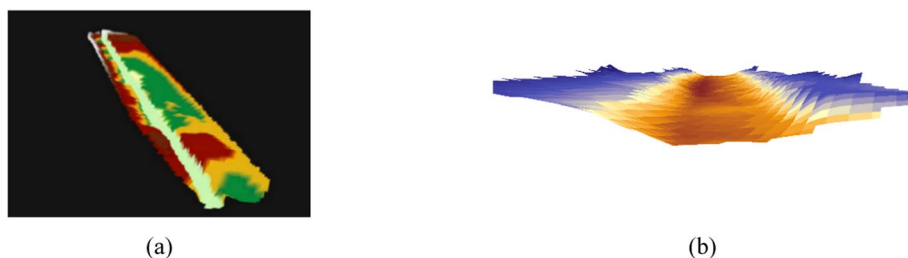


**Fig. 8** **a** The DEM after combining the raw LiDAR-derived DEM and the width and riverbed information. **b** The cross-section of the river from the 3D model

illustrates the river condition at three different water level values, which were 8.8, 9.3, and 12.55 m.

A cross-section of the river is illustrated in Fig. 10. The light blue line represents the water level at 8.80 m during normal conditions. It can be seen that the water surface started to exceed the riverbank at 10.55 m.

From the 3D model, water volume could also be identified by using the estimated water level as the surface Z value. Table 5 shows the total volume of water for the three values of water level that were used. The finding shows that the volume of water increased as the water level increased. It indicates that the proposed procedure could provide a volume of information that is useful for flood management and response.

### 3.4 Development of the GUI for the flood monitoring system

#### 3.4.1 Implementation of the water segmentation task in GUI

Since the proposed segmentation method was proven to be effective, the segmented image underwent a post-processing stage to enhance the water regions and reduce noise. To determine the robustness of the trained model, the proposed algorithm was applied in the GUI to segment a new set of images captured from the study area. The GUI was created to assist in extracting water extent from multiple sources of digital photos, including surveillance images for the water segmentation task.

The input image was loaded into the GUI and then appeared on the right-hand axis (Fig. 10). The 'Segmentation' button was pushed to initiate the segmentation and post-processing procedures. The process of segmenting one image required approximately two seconds to complete. The resulting image was then displayed on the same axis and the user could easily identify the highlighted water region in the image as shown in Appendix A.

The segmented image could also be exported to any file directory in image format, either in JPEG, PNG, or TIF, by pushing the export segmentation image' button. The user could easily save multiple flood scenarios from the same location or various locations and visually identify the fluctuation of the water on-site. The saved images from the study area are presented in Appendix B.

It shows that the trained model could segment Kg. Selisek images regardless of the water level conditions. The segmentation results from the GUI could help the authorities in monitoring the river situation remotely by referring to the water region extent that could

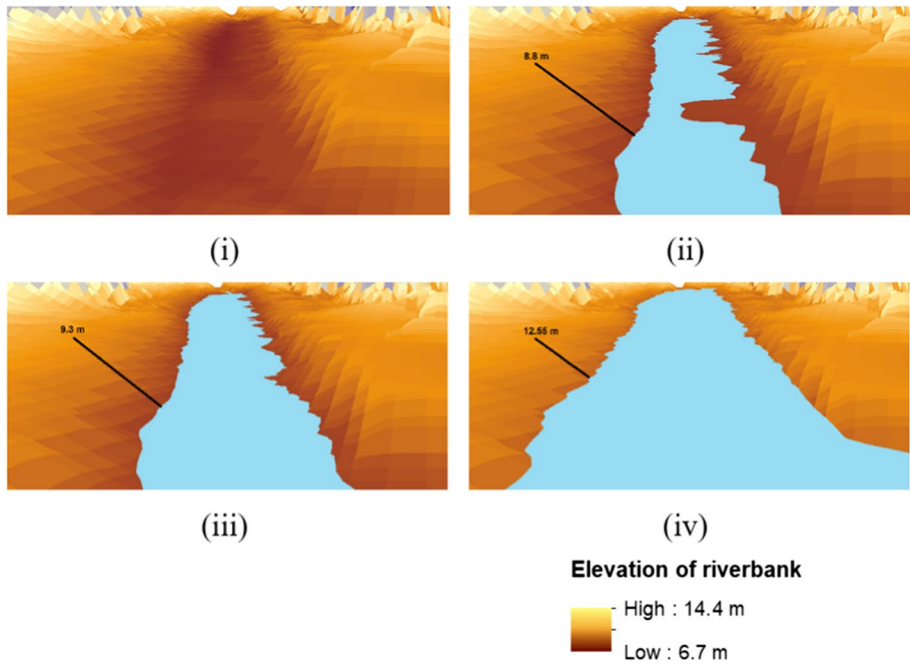


**Fig. 9** The 3D model represents (i) the riverbed (ii) the water level during the normal condition (water level at 8.8 m) (iii) the rising of water at 9.3 m and (iv) the rising of water at 10.55 m

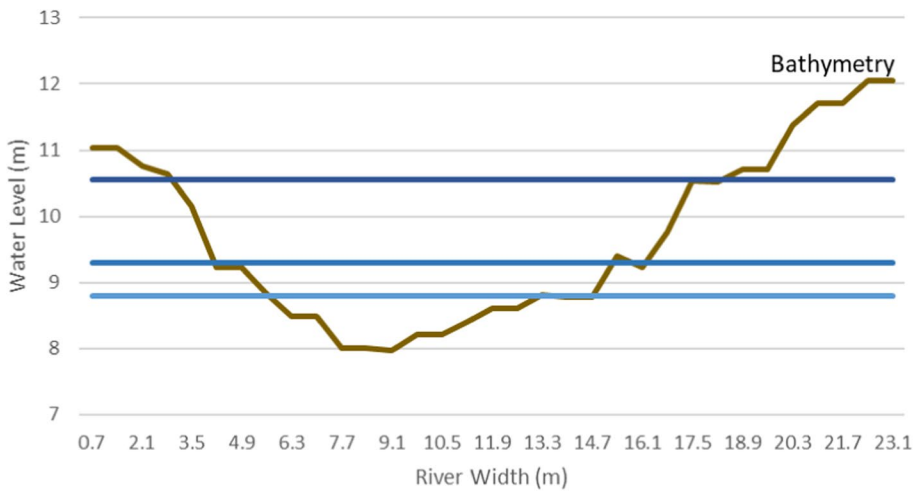


**Fig. 10** A river cross profile with three different water level values



**Table 5** The volume of water obtained from the 3D model and the estimated water level

| Water level (m) | Water volume (m <sup>3</sup> ) |
|-----------------|--------------------------------|
| 8.80            | 421.06                         |
| 9.30            | 1004.56                        |
| 10.55           | 3263.27                        |

be demonstrated visually. With this visual evidence, it is believed that the authorities could gain more confidence to make decisions on flood rescue and operations.

### 3.4.2 Implementation of water level estimation task in the GUI

For the water level estimation procedure in the GUI, the result from the segmentation task could be retrieved by clicking the retrieve button. The location of the particular image was selected in the GUI to provide the correct markers of the specific location for water level computation. Information in terms of the time and date of the input image was also required so that the information could be recorded in the database. Water level estimation was executed when the water level estimation button was pushed. The estimated water level was displayed above the image axis together with its current status, which indicated the severity of the river water level as shown in Appendix C.

Here, the current image could be saved into a directory chosen by the user. Several images saved from the water level estimation procedure are presented in Appendix D. The evolution of the water level could be visually identified and the information was supported by the water level value and its severity status.

Moreover, the estimated value could also be recorded in a database by using the Water level button in the export data panel. The database was saved in a predefined local disk of the user so that multiple water level values could be recorded in the same file. The file contained information such as location, date, time, and water level, as shown in Appendix E. Appendix E shows Excel sheet that contains the information of the image submitted by the user in terms of locations, date, and time as well as the estimated water level values.

By having this kind of information, the authorities could do further analysis such as study the pattern of water fluctuation in particular locations. The information could be plotted into a graph for a better understanding of the water fluctuation. In addition, the water level values could also be used as a backup water level measurement in case unforeseen circumstances occur during flood disasters. The estimated values could be integrated with flood modeling developed by DID to validate the performance of the flood model during flood events. In addition, the output from the segmentation procedure could highlight the water region and visualise the current condition on-site. Hence, it is easier for the civilians to understand the real situation and follow the instructions from the emergency response team and eventually reduce the risk of severe flood impact.

Overall, despite the versatility of the segmentation procedure, which can be applied to images depicting various flood scenarios, a notable limitation of the proposed methodology is its locality-based river water level estimation. This limitation arises from the dependence on specific elevation values corresponding to different areas. To employ the

proposed estimation framework effectively, it becomes necessary to gather elevation data for the particular area of interest.

## 4 Conclusions

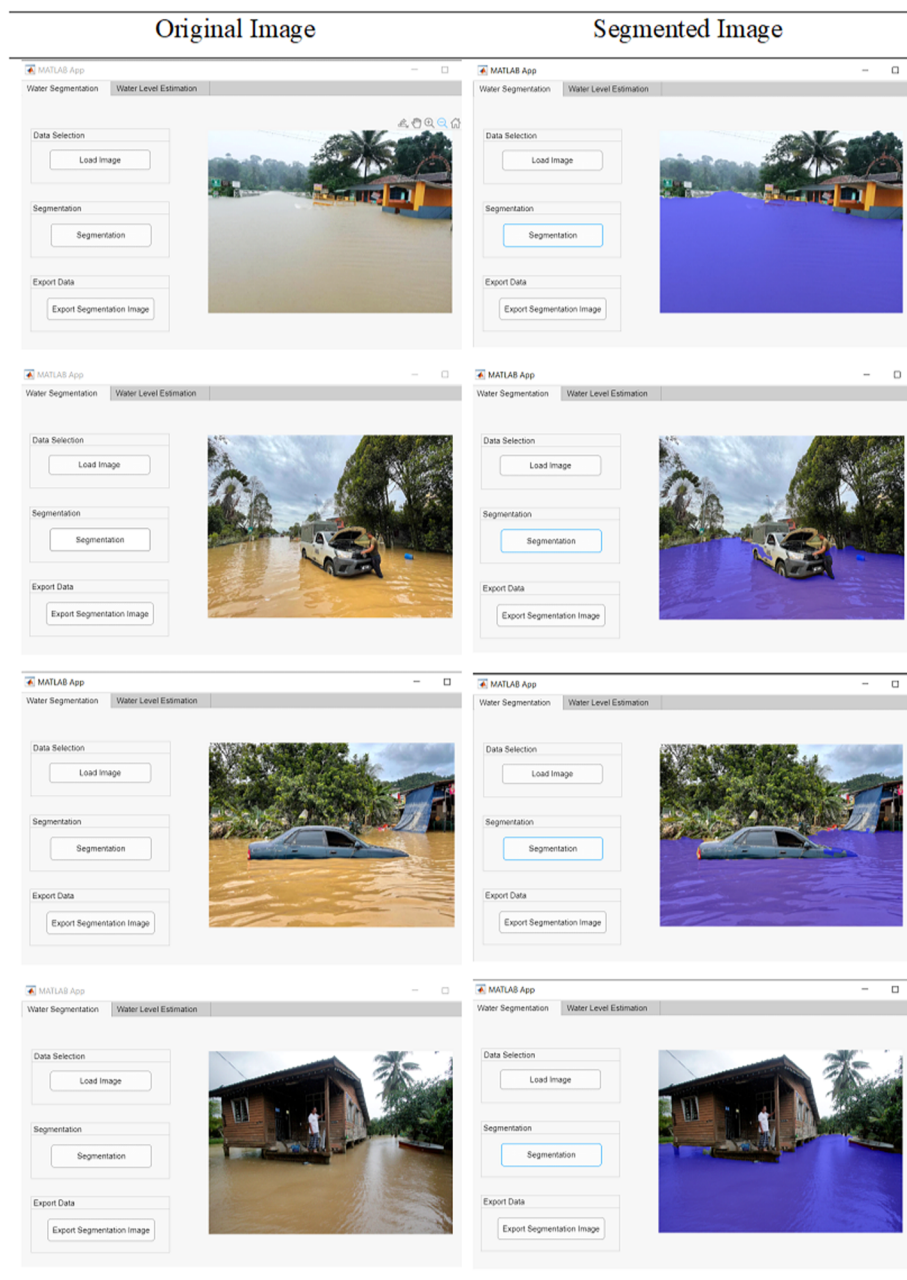
In this study, a state-of-the-art deep learning segmentation approach was used to identify water regions from the surveillance cameras. The deep learning water segmentation was carried out using the DeepLabv3+ network. The results were satisfactory with the IoU metric achieved around 0.95 and the proposed segmentation method was able to segment various water scenes. Meanwhile, the water level procedure is a locality-based approach as it needs elevation information of the specific area to calculate the water levels. The estimated water levels were computed using the segmented image and predefined markers with elevation information that was generated from LiDAR data and then the information was saved into a structured database. The proposed water level estimation was evaluated using Spearman's correlation coefficient, which achieved nearly 0.9, indicating a strong association between both data. The MAE and RMSE for the estimated water levels were 0.01 m and 0.86 m, respectively. Therefore, it can be concluded that the proposed water level procedure can portray the actual water level trends of the river.

In order to have a better representation of the elevation of the river and the fluctuation of water levels, a 3D model was developed by combining the dimensions of the river and the LiDAR data. Using the water level findings from the proposed water level estimation, a flood simulation was conducted to describe the changes in the river water level. The water volume was also calculated using both the 3D model and the estimated water level. The findings show that as the water level rose, so did the volume of water. It suggests that the proposed method could provide volume information that is useful for flood management and rescue operations. Lastly, this work aimed to develop a graphical user interface (GUI) that can extract flood information such as water extent and water level fluctuation from surveillance images during flood events. By having this information, the authorities can make a clear judgement in planning and managing flood-related situations, especially if there is a technical problem with the current practice, which is using the telemetry system. Besides, the result from the GUI is easy to interpret, which can help the citizen to understand and visualise the real situation so that they can comply with the emergency response team's instructions, and ultimately lower the chance of serious flood effects.

The primary objective of this study is to integrate deep learning and lidar data for surveillance camera-based river water level monitoring in flood applications. While the proposed method successfully addresses the main goal, the current results indicate ample room for enhancement. Recommendations for future work include the need for a comprehensive labeled dataset encompassing night-time scenarios to assess the segmentation model's performance in both daylight and nocturnal conditions. Additionally, it is suggested to increase the number of virtual markers for each water level threshold to enhance the accuracy of water level estimation. Exploring alternative approaches, such as incorporating virtual markers based on permanent water level intervals on-site, is also recommended for further refinement of the proposed methodology.

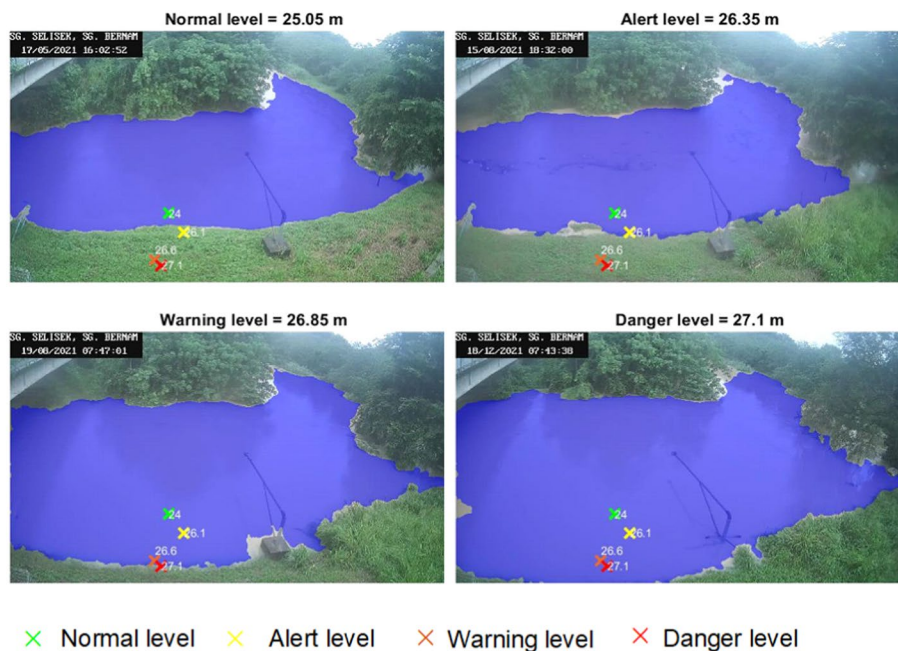
## Appendix A

The screenshot of the execution of the automated procedure for Kampung Selisek using the segmentation procedure of the GUI.



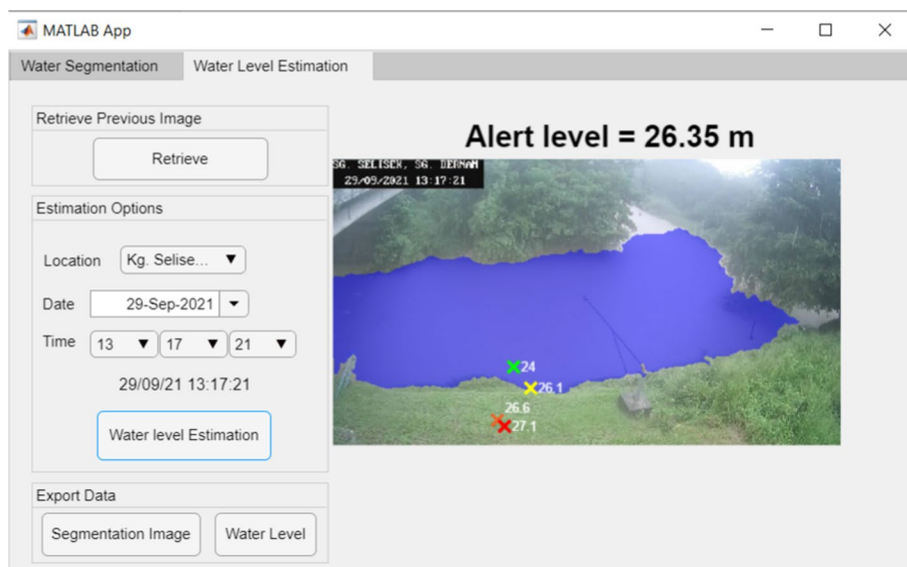
## Appendix B

The segmented images were saved from the execution of the automated procedure for Kampung Selisek.



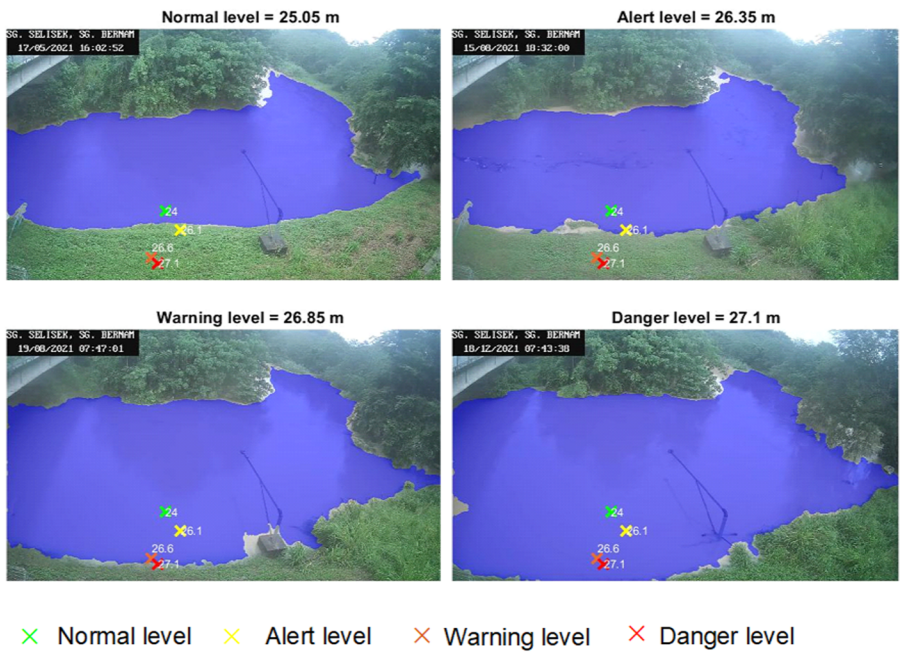
## Appendix C

The result was from the water level estimation procedure in the GUI.



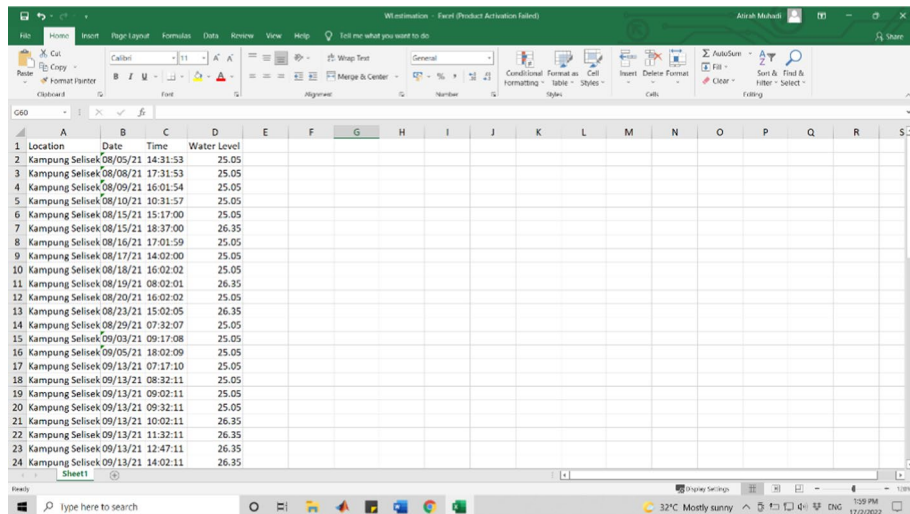
Appendix D

Image saved from the water level estimation procedure that includes the segmented result and water level status.



## Appendix E

Excel sheet that contains the information of image submitted by the user in terms of locations, date, and time as well as the estimated water level values.



| 1  | A               | B        | C        | D           | E | F | G | H | I | J | K | L | M | N | O | P | Q | R | S |
|----|-----------------|----------|----------|-------------|---|---|---|---|---|---|---|---|---|---|---|---|---|---|---|
|    | Location        | Date     | Time     | Water Level |   |   |   |   |   |   |   |   |   |   |   |   |   |   |   |
| 2  | Kampung Selisek | 08/05/21 | 14:31:53 | 25.05       |   |   |   |   |   |   |   |   |   |   |   |   |   |   |   |
| 3  | Kampung Selisek | 08/08/21 | 17:31:53 | 25.05       |   |   |   |   |   |   |   |   |   |   |   |   |   |   |   |
| 4  | Kampung Selisek | 08/09/21 | 16:01:54 | 25.05       |   |   |   |   |   |   |   |   |   |   |   |   |   |   |   |
| 5  | Kampung Selisek | 08/10/21 | 10:31:57 | 25.05       |   |   |   |   |   |   |   |   |   |   |   |   |   |   |   |
| 6  | Kampung Selisek | 08/15/21 | 15:17:00 | 25.05       |   |   |   |   |   |   |   |   |   |   |   |   |   |   |   |
| 7  | Kampung Selisek | 08/15/21 | 18:37:00 | 26.35       |   |   |   |   |   |   |   |   |   |   |   |   |   |   |   |
| 8  | Kampung Selisek | 08/16/21 | 17:01:59 | 25.05       |   |   |   |   |   |   |   |   |   |   |   |   |   |   |   |
| 9  | Kampung Selisek | 08/17/21 | 14:02:00 | 25.05       |   |   |   |   |   |   |   |   |   |   |   |   |   |   |   |
| 10 | Kampung Selisek | 08/18/21 | 16:02:02 | 25.05       |   |   |   |   |   |   |   |   |   |   |   |   |   |   |   |
| 11 | Kampung Selisek | 08/19/21 | 08:02:01 | 26.35       |   |   |   |   |   |   |   |   |   |   |   |   |   |   |   |
| 12 | Kampung Selisek | 08/20/21 | 16:02:02 | 25.05       |   |   |   |   |   |   |   |   |   |   |   |   |   |   |   |
| 13 | Kampung Selisek | 08/23/21 | 15:02:05 | 26.35       |   |   |   |   |   |   |   |   |   |   |   |   |   |   |   |
| 14 | Kampung Selisek | 08/29/21 | 07:32:07 | 25.05       |   |   |   |   |   |   |   |   |   |   |   |   |   |   |   |
| 15 | Kampung Selisek | 09/03/21 | 09:17:08 | 25.05       |   |   |   |   |   |   |   |   |   |   |   |   |   |   |   |
| 16 | Kampung Selisek | 09/05/21 | 18:02:09 | 25.05       |   |   |   |   |   |   |   |   |   |   |   |   |   |   |   |
| 17 | Kampung Selisek | 09/13/21 | 07:17:10 | 25.05       |   |   |   |   |   |   |   |   |   |   |   |   |   |   |   |
| 18 | Kampung Selisek | 09/13/21 | 08:32:11 | 25.05       |   |   |   |   |   |   |   |   |   |   |   |   |   |   |   |
| 19 | Kampung Selisek | 09/13/21 | 09:02:11 | 25.05       |   |   |   |   |   |   |   |   |   |   |   |   |   |   |   |
| 20 | Kampung Selisek | 09/13/21 | 09:32:11 | 25.05       |   |   |   |   |   |   |   |   |   |   |   |   |   |   |   |
| 21 | Kampung Selisek | 09/13/21 | 10:02:11 | 26.35       |   |   |   |   |   |   |   |   |   |   |   |   |   |   |   |
| 22 | Kampung Selisek | 09/13/21 | 11:32:11 | 26.35       |   |   |   |   |   |   |   |   |   |   |   |   |   |   |   |
| 23 | Kampung Selisek | 09/13/21 | 12:47:11 | 26.35       |   |   |   |   |   |   |   |   |   |   |   |   |   |   |   |
| 24 | Kampung Selisek | 09/13/21 | 14:02:11 | 26.35       |   |   |   |   |   |   |   |   |   |   |   |   |   |   |   |

**Acknowledgements** This study was funded by Universiti Putra Malaysia under the Putra Grant, GP-IPM (Grant number: 9780100). Besides, the authors would like to appreciate the given opportunity to collaborate with the European Union under the RECONNECT project funded by the European's Union Horizon 2020 (Project ID: 776866). The authors also appreciate the support for this study from the Faculty of Engineering and the Institute of Aquaculture and Aquatic Sciences, Universiti Putra Malaysia. Lastly, the authors would like to thank the Department of Irrigation and Drainage for publicly sharing the surveillance images and water level data.

**Open research** Input dataset are publicly available at the Zenodo data repository (Nur Atirah Muhadi 2022).

**Author contributions** All authors contributed to the study conception and design. NAM and AFA have designed and conducted the research in collaboration with SKB and MRM, supervised by AM and ZV. NAM has written the manuscript with contributions from all co-authors.

**Funding** This study was funded by GP-IPM, Universiti Putra Malaysia (Grant number: 9780100). Besides, the authors would like to appreciate the given opportunity to collaborate with the European Union under the RECONNECT project funded by the Europeans Union Horizon 2020 (Project ID: 776866).

## Declarations

**Competing interests** The authors have no relevant financial or non-financial interests to disclose.

## References

- Akiyama TS, Marcato Junior J, Gonçalves WN, Bressan PO, Eltner A, Binder F, Singer T (2020) Deep learning applied to water segmentation. *Int Arch Photogramm Remote Sens Apat Inf Sci XLIII-B2-2(B2):1189–1193*. <https://doi.org/10.5194/isprs-archives-XLIII-B2-2020-1189-2020>




- Arshad B, Ogie R, Barthelemy J, Pradhan B, Verstaavel N, Perez P (2019) Computer vision and iot-based sensors in flood monitoring and mapping: a systematic review. *Sensors (switzerland)* 19(22):1–28. <https://doi.org/10.3390/s19225012>
- CFE-DM (2019) Malaysia disaster management reference handbook. Center for Excellence in Disaster & Humanitarian Assistance (CFE-DM). Retrieved from <http://reliefweb.int/map/chile/chilelocation-map-2013>
- Costa DG, Guedes LA, Vasques F, Portugal P (2013) Adaptive monitoring relevance in camera networks for critical surveillance applications. *Int J Distrib Sensor Netw*. <https://doi.org/10.1155/2013/836721>
- Costabile P, Costanzo C, De Lorenzo G, De Santis R, Penna N, Macchione F (2021) Terrestrial and airborne laser scanning and 2-D modelling for 3-D flood hazard maps in urban areas: new opportunities and perspectives. *Environ Model Softw* 135:104889. <https://doi.org/10.1016/j.envsoft.2020.104889>
- DID (2018) Hydrological standard for water level station instrumentation. Kuala Lumpur, Malaysia: Department of Irrigation and Drainage (DID) Malaysia
- Eltner A, Bressan PO, Akiyama T, Gonçalves WN, Marcato Junior J (2021) Using deep learning for automatic water stage measurements. *Water Resour Res*. <https://doi.org/10.1029/2020WR027608>
- Fernandez-Moral E, Martins R, Wolf D, Rives P (2018) A new metric for evaluating semantic segmentation: leveraging global and contour accuracy. In: IEEE intelligent vehicles symposium, proceedings, 2018–June(March 2021), pp 1051–1056. <https://doi.org/10.1109/IVS.2018.8500497>
- Lo S-WW, Wu J-HH, Lin F-PP, Hsu C-HH (2015a) Cyber surveillance for flood disasters. *Sensors (switzerland)* 15(2):2369–2387. <https://doi.org/10.3390/s150202369>
- Lo SW, Wu JH, Lin FP, Hsu CH (2015b) Visual sensing for urban flood monitoring. *Sensors (switzerland)* 15(8):20006–20029. <https://doi.org/10.3390/s150820006>
- Lopez-Fuentes L, Rossi C, Skinnemoen H (2017) River segmentation for flood monitoring. In: Proceedings - 2017 IEEE International Conference on Big Data, Big Data 2017 (vol 2018-Janua, pp 3746–3749). <https://doi.org/10.1109/BigData.2017.8258373>
- Moy de Vitry M, Kramer S, Dirk Wegner J, Leitao JP (2019a) Scalable flood level trend monitoring with surveillance cameras using a deep convolutional neural network. *Hydrol Earth Syst Sci* 23(11):4621–4634. <https://doi.org/10.5194/hess-23-4621-2019>
- Moy de Vitry M, Kramer S, Wegner JD, Leitão JP (2019b) Scalable flood level trend monitoring with surveillance cameras using a deep convolutional neural network. *Hydrol Earth Syst Sci Discuss*. <https://doi.org/10.5194/hess-2018-570>
- Muhadi NA, Abdullah AF, Bejo SK, Mahadi MR, Mijic A (2020) Image segmentation methods for flood monitoring system. *Water* 12(6):1825. <https://doi.org/10.3390/w12061825>
- Muhadi NA, Abdullah AF, Bejo SK, Mahadi MR, Mijic A (2021) Deep learning semantic segmentation for water level estimation using surveillance camera. *Appl Sci (switzerland)*. <https://doi.org/10.3390/app11209691>
- Mynett AE, Vojinovic Z (2009) Hydroinformatics in multi-colours-part red: Urban flood and disaster management. *J Hydroinf* 11(3–4):166–180. <https://doi.org/10.2166/hydro.2009.027>
- Muhadi NA. (2022). Dataset For Water Segmentation [Data set]. In *Deep Learning Semantic Segmentation for Water Level Estimation Using Surveillance Camera* (Vol. 11, Number 20, p. 9691). Zenodo. <https://doi.org/10.5281/zenodo.7269522>
- Oddo PC, Bolten JD (2019) The value of near real-time earth observations for improved flood disaster response. *Front Environ Sci* 7(September):1–11. <https://doi.org/10.3389/fenvs.2019.00127>
- Price RK, Vojinovic Z (2008) Urban food disaster management. *Urban Water J* 5(3):259–276. <https://doi.org/10.1080/15730620802099721>
- Sathish Kumar D, Arya DS, Vojinovic Z (2013) Modeling of urban growth dynamics and its impact on surface runoff characteristics. *Comput Environ Urban Syst* 41:124–135. <https://doi.org/10.1016/j.compenvurbsys.2013.05.004>
- Spearman C (1904) The proof and measurement of association between two things. *Am J Psychol* 15(1):72–101. <https://doi.org/10.1037/h0065390>
- UNDRR (2020) The human cost of disasters - an overview of the last 20 years 2000–2019. Human Cost of Disasters. <https://doi.org/10.18356/79b92774-en>
- Vandaele, Remy, Dance SL, Ojha V (2021) Deep learning for the estimation of water-levels using river cameras. *Hydrol Earth Syst Sci Discuss* (February) 1–28
- Vandaele, Rémy, Dance SL, Ojha V (2021) Automated water segmentation and river level detection on camera images using transfer learning. *Lecture Notes in Computer Science (Including Subseries Lecture Notes in Artificial Intelligence and Lecture Notes in Bioinformatics)* 12544 LNCS(March):232–245. [https://doi.org/10.1007/978-3-030-71278-5\\_17](https://doi.org/10.1007/978-3-030-71278-5_17)

Witherow MA, Sazara C, Winter-Arboleda IM, Elbakary MI, Cetin M, Iftekharruddin KM (2018) Flood-water detection on roadways from crowdsourced images. *Comput Methods Biomec Biomed Eng: Imaging Visual* 1163:1–12. <https://doi.org/10.1080/21681163.2018.1488223>

**Publisher's Note** Springer Nature remains neutral with regard to jurisdictional claims in published maps and institutional affiliations.

Springer Nature or its licensor (e.g. a society or other partner) holds exclusive rights to this article under a publishing agreement with the author(s) or other rightsholder(s); author self-archiving of the accepted manuscript version of this article is solely governed by the terms of such publishing agreement and applicable law.

## Authors and Affiliations

**Nur Atirah Muhadi**<sup>1,2</sup>  · **Ahmad Fikri Abdullah**<sup>1,2,3</sup> · **Siti Khairunniza Bejo**<sup>1,2,4</sup> · **Muhammad Razif Mahadi**<sup>1,2</sup> · **Ana Mijic**<sup>5</sup> · **Zoran Vojinovic**<sup>6</sup>

✉ Nur Atirah Muhadi  
[nuratirah@upm.edu.my](mailto:nuratirah@upm.edu.my)

<sup>1</sup> Department of Biological and Agricultural Engineering, Faculty of Engineering, Universiti Putra Malaysia, 43400 Serdang, Selangor, Malaysia

<sup>2</sup> Smart Farming Technology Research Centre (SFTRC), Universiti Putra Malaysia, 43400 Serdang, Selangor, Malaysia

<sup>3</sup> Institute of Aquaculture and Aquatic Sciences, Batu 7, Jalan Kemang 6, Teluk Kemang, 71050 Si Rusa, Port Dickson, Negeri Sembilan, Malaysia

<sup>4</sup> Institute of Plantation Studies (IKP), Universiti Putra Malaysia, 43400 Serdang, Selangor, Malaysia

<sup>5</sup> Department of Civil and Environmental Engineering, Imperial College London, South Kensington Campus, London SW7 2AZ, UK

<sup>6</sup> IHE Delft Institute for Water Education, Westvest 7, 2611 AX Delft, The Netherlands